

**Cell Reports, Volume 19**

## **Supplemental Information**

### **An Integrative Framework Reveals**

### **Signaling-to-Transcription Events**

### **in Toll-like Receptor Signaling**

**Philipp Mertins, Dariusz Przybylski, Nir Yosef, Jana Qiao, Karl Clauser, Raktima Raychowdhury, Thomas M. Eisenhaure, Tanja Maritzen, Volker Haucke, Takashi Satoh, Shizuo Akira, Steven A. Carr, Aviv Regev, Nir Hacohen, and Nicolas Chevrier**

Figure S1

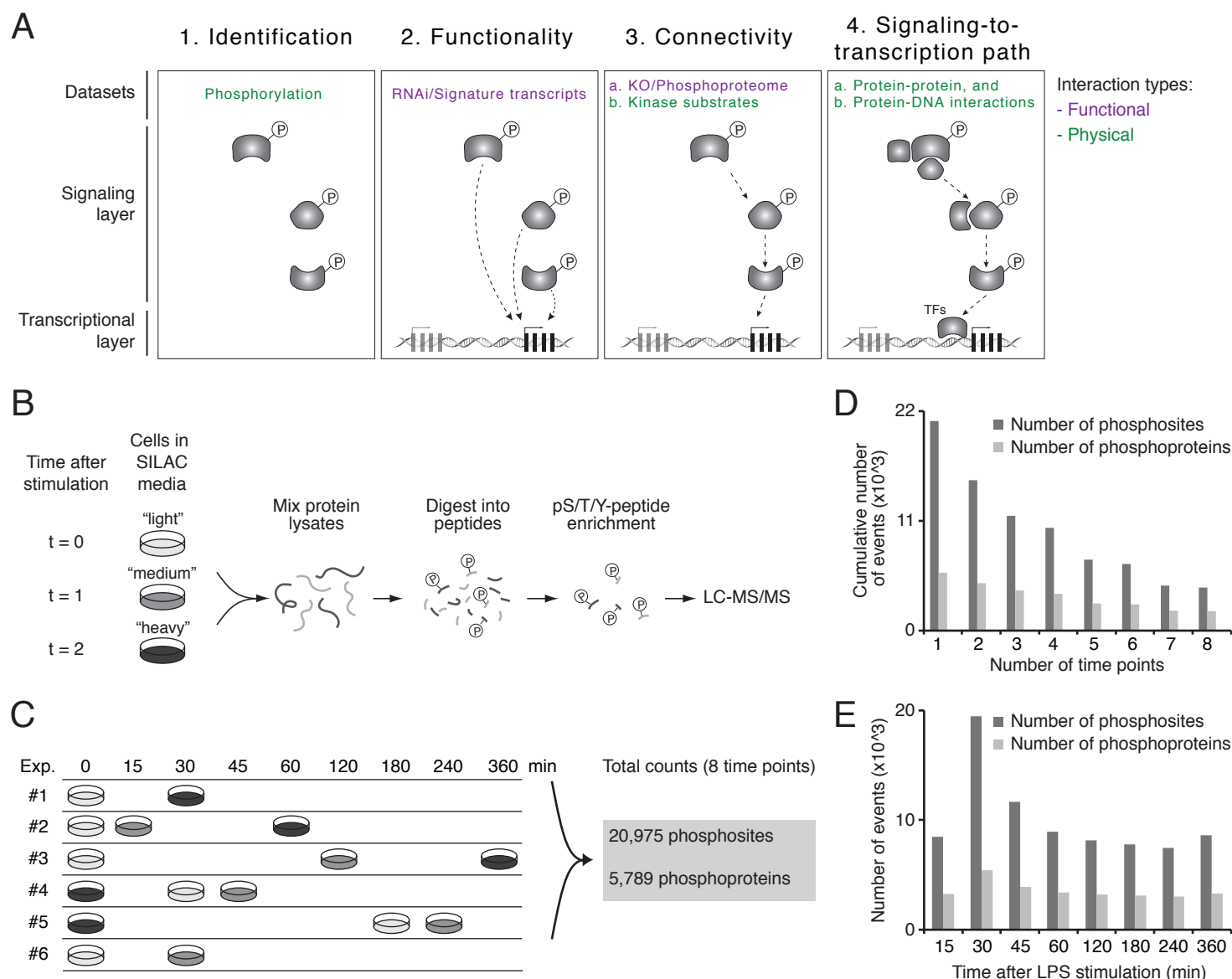


**Figure S1. Overview of the experimental design and outcome of temporal phosphoproteomic profiling of TLR4-stimulated DCs, Related to Figure 1.**

(A) Diagram highlighting the general steps of our integrative approach that includes the identification of temporal changes in phosphorylation (1), functional testing using genetic perturbations (2), connecting kinases and substrates (3), and inferring biochemical paths linking signaling to transcription events (4). All these steps rely on data capturing physical and functional interactions in mouse primary DCs stimulated with LPS.

(B) Schematic depiction of the experimental workflow for phosphoproteomics. From left: Protein lysates from unstimulated (t = 0) and LPS-treated cells (t = 1 and 2) grown in "light", "medium" or "heavy" SILAC media were mixed (1:1:1) and digested into peptides with trypsin before phospho-serine, -threonine, and -tyrosine (pS/T/Y) peptide enrichment using immobilized metal affinity chromatography (IMAC), and LC-MS/MS analysis (see Experimental Procedures).

(C) Schematic summary of the temporal phosphoproteomic profiling. Six experiments were conducted (from top to bottom) to cover control and stimulated cells (top, 8 time points post-LPS stimulation) with SILAC label switching as indicated with the colored-dishes matching the nomenclature from B. Total counts of phosphosites and phosphoproteins detected across all time points are indicated on the right.

(D-E) Distributions of phosphosites and phosphoproteins detected across multiple (cumulative counts; D) and individual time points (E).

Figure S2

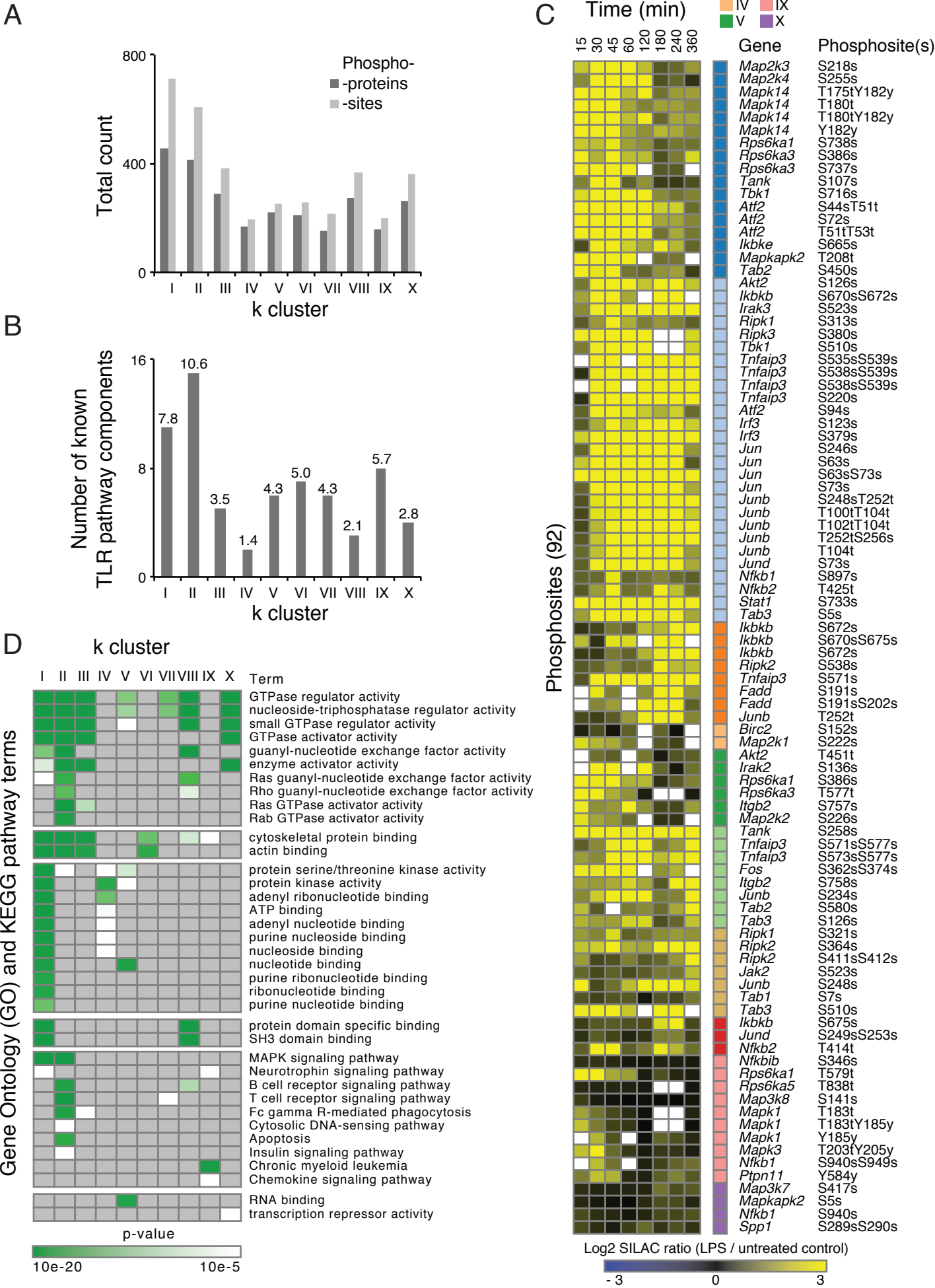


**Figure S2. Dynamic phosphoproteomic profiles reveal phosphosites regulated on known TLR components and differential pathway enrichment over time, Related to Figure 2.**

(A-B) Distributions of phosphosites and phosphoproteins (A; Y axis), and known TLR pathway proteins (B; Y axis) detected across the 10 k-means clusters from Figure 1A (X axis). Numbers on top of each bar indicate the percent of known TLR proteins within each cluster (B).

(C) Phosphorylation profiles of known TLR pathway proteins. Log2 fold changes between LPS-treated and untreated cells for 92 phosphosites on known TLR proteins (rows) detected in at least 6 out of 8 time points (columns). Phosphosites are partitioned into 10 clusters using k-means (legend, top; color bars, right). Right, gene names and phosphosites localization (S, serine; T, threonine; Y, tyrosine). White indicates missing values.

(D) Gene enrichment analysis of LPS-dependent phosphoproteins. Enrichment p-values (modified Fisher's exact test, showing values  $< 10^{-5}$ ; grey boxes indicate values above this cutoff) for Gene Ontology (GO) and KEGG pathway terms (rows; term name indicated on the right) across all 10 k-means clusters (columns).

Figure S3



**Figure S3. Genetic perturbation profiles of the 131 phosphoproteins selected from phosphoproteomic profiles, Related to Figure 3.**

(A-B) Candidate filtering and associated gene enrichment analysis of LPS-dependent phosphoproteins selected for functional analysis. Enrichment p-values (modified Fisher's exact test, showing values  $< 10^{-5}$ ; grey boxes indicate values above this cutoff) for Gene Ontology (GO) and KEGG pathway terms (rows; term name indicated on the right) across all 3 filters for candidate gene selection (columns).

(C) Perturbation profiles of 131 phosphoproteins. Shown are the perturbed candidates and control genes (columns) and the log2 fold changes between gene-specific and control shRNAs (rows) of 263 target genes (including control targets used as "housekeeping", unchanged genes for normalization). The right-most column categorizes target genes into controls (dark green), and antiviral (light green) and inflammatory (light orange) programs. Top, bar plot indicating knockdown efficiency for each perturbed gene (top left, percentage of remaining mRNA transcripts for indicated genes upon knockdown).

Figure S4

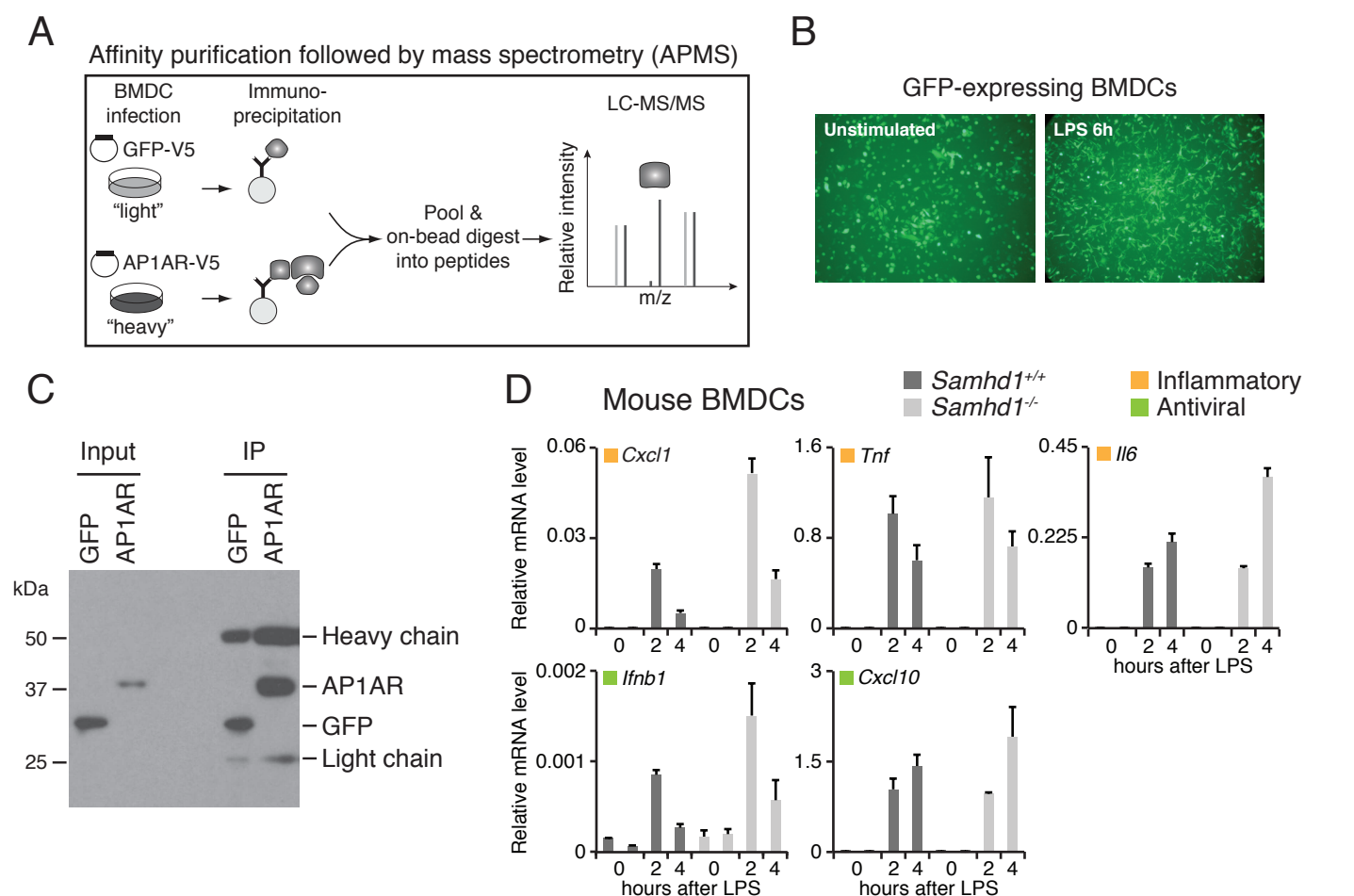


**Figure S4. A method for affinity-purification followed by MS (AP-MS) in BMDCs, and analysis of *Samhd1*<sup>-/-</sup> mouse BMDCs, Related to Figure 4.**

(A) Diagram depicting our experimental approach for AP-MS in mouse BMDCs.

(B) BMDCs overexpressing V5-tagged proteins through lentiviral infection respond normally to LPS. Micrographs of GFP-expressing DCs before and after LPS stimulation.

(C) Immunoblot analysis of input and immunoprecipitated (IP) samples from DCs expressing V5-GFP or V5-AP1AR.

(D) Expression levels (relative to Gapdh; qPCR) of indicated inflammatory (light orange) and antiviral (light green) cytokines in *Samhd1*<sup>+/+</sup> and *Samhd1*<sup>-/-</sup> BMDCs stimulated with LPS for 2 and 4 h or left untreated as control (duplicate wells are shown).

Figure S5

Correlation of knockdown profiles with TF binding

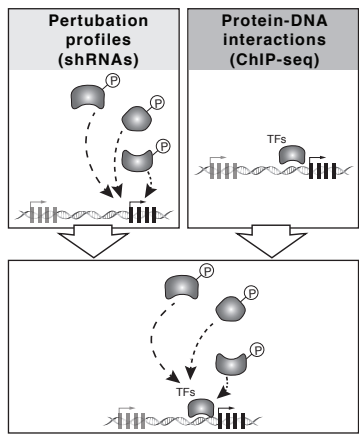


**Figure S5. Measuring overlaps between knockdown profiles and TF binding sites, Related to Figure 5.**

Diagram depicting overlaps between genes affected by knockdown and genes whose promoters are bound by a given transcription factor (TF), as a schematic example of the analysis performed in Figure 5B.



Figure S6

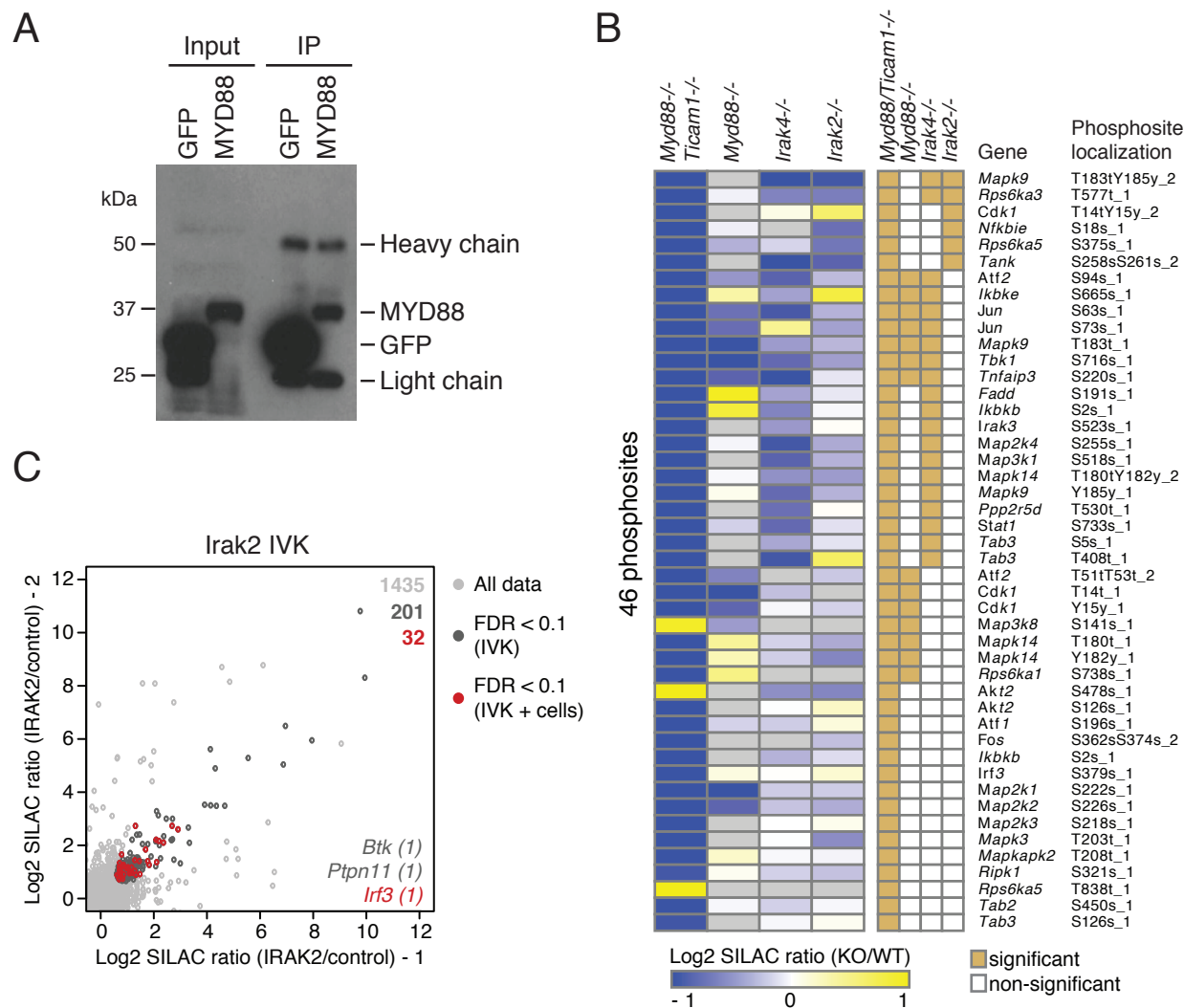


**Figure S6. Physical and functional proteomics assays pinpoint how phosphorylation of known TLR pathway regulators is modulated by KO, Related to Figure 6.**

(A) Immunoblot analysis of input and immunoprecipitated (IP) samples from DCs expressing V5-GFP or V5-MYD88.

(B) Phosphoproteomics in KO cells. Left, shown is a heatmap for SILAC ratios of phosphosites (rows) in 4 KO models (columns) at 30 min after LPS stimulation compared to control wild-type cells, as indicated (grey, missing values). Middle, shown in light brown are phosphosites with significant up- or down-regulation in KO vs WT. Right, shown are the 46 phosphosites mapping to known TLR signaling regulators (Letters on the right indicated the phosphorylated residue: S, serine; T, threonine; Y, tyrosine). Numbers indicated the amino-acid position in the protein).

(C) In vitro kinase (IVK) assay followed by phosphoproteomics. Shown are dot plots of SILAC ratios of phosphosites identified using purified IRAK2. Light grey, all data points; dark grey, phosphosites with FDR < 0.1 in IVK; red, phosphosites with FDR < 0.1 in both IVK and in cells stimulated with LPS, which highlights the overlap between IVK and phosphoproteome measurements on stimulated cells (denoted as IVK + cells). Gene names at the bottom right of the plot indicates known TLR components with the number of phosphosites in parenthesis.

Figure S7

A Summary of data collected in BMDCs on physical and functional interactions

	Datasets	Measurements	Matching figures
Physical interactions	Phosphorylation	Phosphoproteomics	Figure 1C
	Large-scale IVK	Phosphoproteomics	Figure 6F, 6G, and S6C
	Protein-protein interactions	AP-MS	Figure 4D, 6A, and 6B
	Protein-DNA interactions	TF ChIP-seq	Figure 5B
Functional interactions	shRNA / Signature transcripts	Multiplex mRNA counting	Figure 3B and S3C
	KO / Phosphoproteome	Phosphoproteomics	Figure 6D

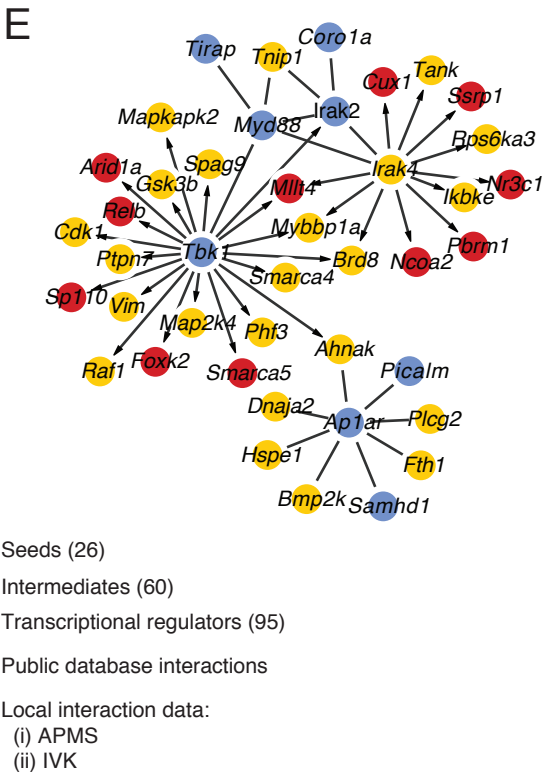
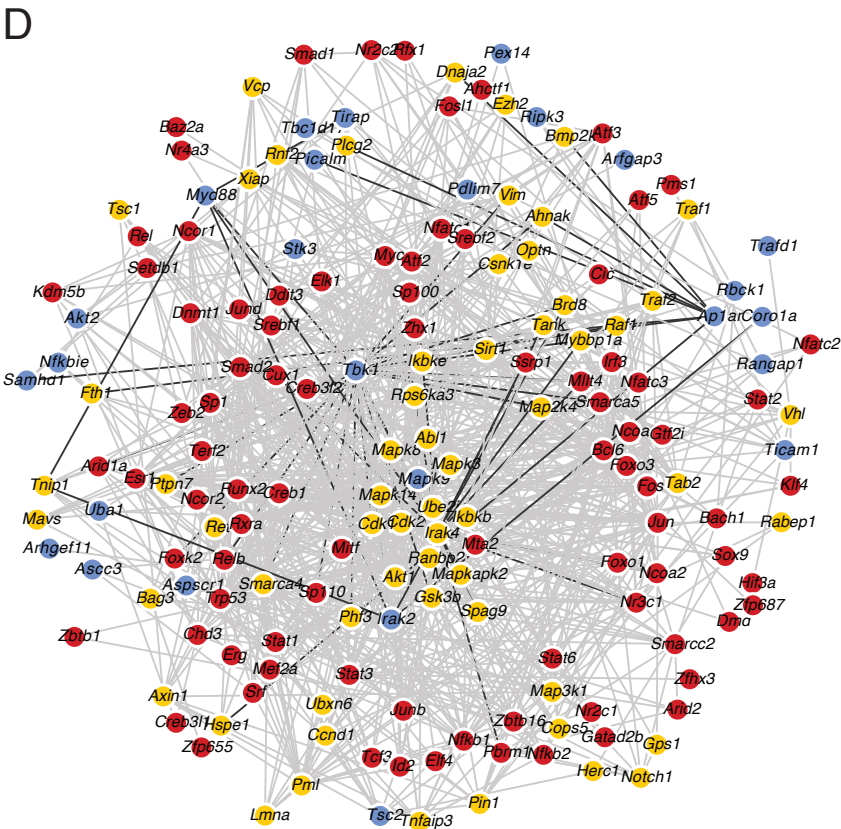
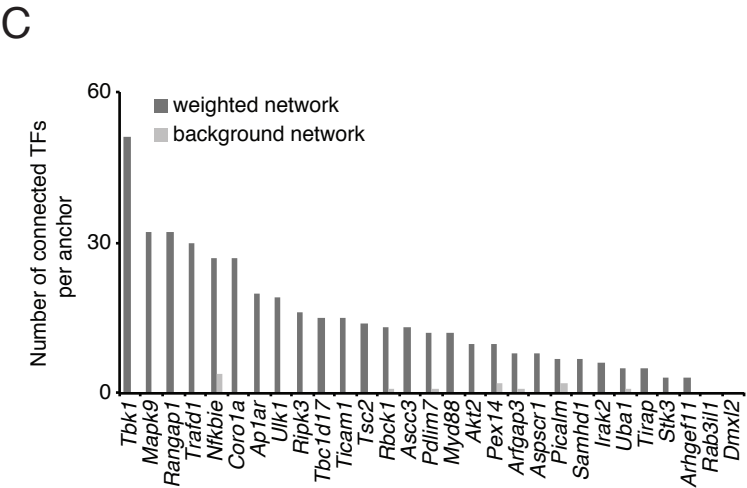
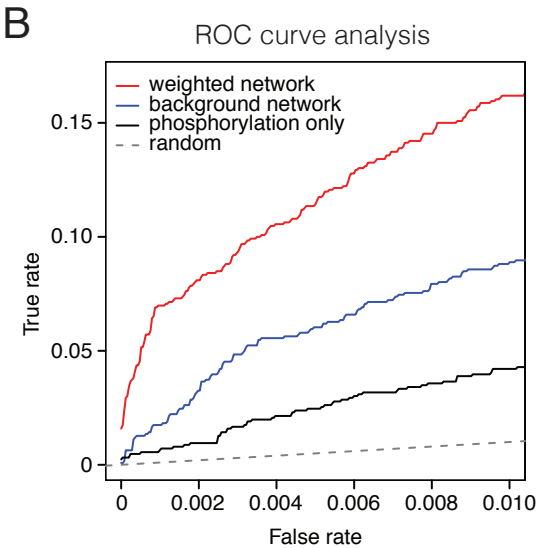


**Figure S7. An integrative analysis reveals signaling-to-transcription paths in the TLR4 system, Related to Figure 7.**

(A) List summarizing the physical and functional interaction data sets collected in the cellular context of BMDCs stimulated with LPS.

(B) Receiver operator characteristic (ROC) analysis demonstrates the ability of our integrative algorithm to retrieve known seed-target node relationships between canonical TLR pathway components.

(C) Total number of transcription regulators (TRs) for which significant relationships were found with the 29 'seed' nodes using 'weighted network' (dark grey) and 'background network' (light grey) methods.

(D) An interaction network connects 27 seeds (blue) to 95 transcriptional regulators (red) through the top 60 intermediate (yellow) nodes. Shown is a close-up view of the network from Figure 7E depicting protein names on nodes and edge types (database, AP-MS, and/or IVK).

(E) Sub-network extracted from panel D showing interactions from local data sets as dark edges (AP-MS, undirected; IVK, directed).

## SUPPLEMENTAL EXPERIMENTAL PROCEDURES

### Cells

Bone marrow-derived dendritic cells (BMDCs) were generated from 6-8 week old female C57BL/6J (Jackson Laboratories), *Ap1ar*<sup>-/-</sup> (Maritzen et al., 2012), *Samhd1*<sup>-/-</sup> (Rehwinkel et al., 2013), *Myd88*<sup>-/-</sup>, *Myd88*<sup>-/-</sup>/*Ticam*<sup>-/-</sup>, *Irak2*<sup>-/-</sup>, *Irak4*<sup>-/-</sup> mice. Bone marrow cells were collected from femora and tibiae and plated at 10<sup>6</sup> cells/mL on non-tissue culture treated petri dishes or 96-well plates in RPMI-1640 medium (Gibco), supplemented with 10% FBS, L-glutamine, penicillin/streptomycin, MEM non-essential amino acids, HEPES, sodium pyruvate,  $\beta$ -mercaptoethanol, and murine GM-CSF (15 ng/mL; Peprotech). GM-CSF-derived BMDCs were used directly for all RNAi experiments. For all other experiments, floating cells from GM-CSF cultures were sorted at day 5 by MACS using the CD11c (N418) MicroBeads kit (Miltenyi Biotec), or used directly at day 8. Sorted CD11c<sup>+</sup> or floating cells were used as GM-CSF-derived BMDCs, and plated at 10<sup>6</sup> cells/mL and stimulated at 16 h post sorting or collection. Human fibroblasts used in this study were AGS128 SI (c.445C>T p.Gln149\* hom, referred to as M1), AGS495 SA (c.1609-1G>C hom, referred to as M2), and F10Y, F8Y, and PBX2 are controls (referred to as H1-3), and were maintained in DMEM supplemented with 10% FBS. All cell stimulations were performed using ultra-pure *E. coli* K12 LPS (lipopolysaccharide) from Invivogen at 100 ng/mL for indicated times.

### mRNA isolation

Total RNA was extracted with QIAzol reagent following the miRNeasy kit's procedure (Qiagen), and reverse transcribed with the High Capacity cDNA Reverse Transcription kit (Applied

Biosystems). For experiments with more than 12 samples, we harvested PolyA<sup>+</sup> RNA in 96- or 384-well plates with the Turbocapture mRNA kit (Qiagen) and reverse transcribed with the Sensiscript RT kit (Qiagen).

### **qPCR measurements**

Real time quantitative PCR reactions were performed on the LightCycler 480 system (Roche) with FastStart Universal SYBR Green Master Mix (Roche). Every reaction was run in triplicate and GAPDH levels were used as an endogenous control for normalization.

### **shRNA knockdowns**

High titer lentiviruses encoding shRNAs targeting genes of interest were obtained from The RNAi Consortium (TRC; Broad Institute, Cambridge, MA, USA). Bone marrow cells were infected with lentiviruses as described (Chevrier et al., 2011). For each gene of interest, we tested five shRNAs for knockdown efficiency using qPCR of the target gene and selected shRNAs with best knockdown efficacy (typically >75%).

### **mRNA counting and data analysis**

$5 \times 10^4$  bone marrow-derived DCs were lysed in RLT buffer (Qiagen) with 1%  $\beta$ -ME. 10% of the lysate was used for mRNA counting using the nCounter Digital Analyzer (NanoString) and a custom CodeSet constructed to detect a total of 267 genes (including 16 control genes whose expression remain unaffected by TLR stimulation). We normalize data by dividing the nCounter mRNA count values for each gene by the sum of counts obtained for the 16 control genes present in our custom CodeSet. To determine significantly affected signature genes, a fold-change ratio is

computed for each pairwise comparison of a knockdown sample versus a set of control samples (i.e., non-targeting shRNA; at least 10 per experimental batch). As a threshold, we require a substantial fold-change (above a threshold value  $t$ ) in the same direction (up- or down-regulation) in more than half of the pairwise comparisons sample vs. control shRNA. The threshold value  $t$  is determined as  $\max(q, d)$ ,  $d$  being the mean + 1.645 times the standard deviation in the fold change shown by the control genes (corresponding  $\text{top} = 0.05$ , under the assumption of normality). The threshold  $q$  is similar for all comparisons and is based on the noise level estimated from the control shRNA samples. Specifically, we compute gene expression fold changes in all possible pairs of control shRNA samples (which are supposed to be consistent). We set the threshold  $q$  such that 95% of the comparisons exhibit lower fold change than  $q$ . The resulting value of  $q$  is 1.961. Notably, we ignore all pairwise comparisons in which both control and knockdown samples had low counts before normalization ( $<50$ ). All heatmaps and distance matrix analyses were generated using the software Gene-E (<https://software.broadinstitute.org/GENE-E/index.html>).

### **Metabolic labeling of cells**

For stable isotope labeling of amino acids in cell culture (SILAC) experiments, GM-CSF-derived BMDCs were grown for seven days in media containing either normal L-arginine (Arg-0) and L-lysine (Lys-0) (Sigma), L-arginine  $^{13}\text{C}_6$  (Arg-6) and L-lysine D4 (Lys-4), or L-arginine  $^{13}\text{C}_6$ - $^{15}\text{N}_4$  (Arg-10) and L-lysine  $^{13}\text{C}_6$ - $^{15}\text{N}_2$  (Lys-8) (Sigma Isotec). Concentrations for L-arginine and L-lysine were 42 mg/L and 73 mg/L, respectively. To prevent metabolic conversion of L-arginine to L-proline we added 200 mg/L L-proline to the cell culture medium. The cell culture media, Roswell Park Memorial Institute-1640 (RPMI) deficient in L-arginine and L-lysine, was a custom media preparation from Caisson Laboratories (North Logan, UT) and dialyzed serum was

obtained from SAFC-Sigma. We followed all standard SILAC media preparation and labeling steps as previously described (Chevrier et al., 2011).

### **Global serine, threonine, and tyrosine phosphorylation analysis for LPS time course experiments**

BMDCs grown in SILAC media were stimulated with LPS, and lysed and processed for enrichment of phosphopeptides as described previously (Chevrier et al., 2011; Mertins et al., 2013). Briefly, after LPS stimulation, cells grown in non-TC treated Petri dishes were placed on ice and scraped. Cell suspensions were washed in ice-cold PBS and sedimented by centrifugation at 4°C and 1,000 g for 5 minutes. The supernatant was removed and cell pellets were immediately frozen in liquid nitrogen. Cell pellets were lysed for 20 minutes in ice-cold lysis buffer containing 8 M Urea, 75 mM NaCl, 50 mM Tris pH 8.0, 1 mM EDTA, 2 µg/ml Aprotinin (Sigma, A6103), 10 µg/ml Leupeptin (Roche, #11017101001), 1 mM PMSF, 10 mM NaF, 2 mM Na<sub>3</sub>VO<sub>4</sub>, 50 ng/ml Calyculin A (Calbiochem, #208851), Phosphatase inhibitor cocktail 1 (1/100, Sigma, P2850) and Phosphatase inhibitor cocktail 2 (1/100, Sigma, P5726). Lysates were pre-cleared by centrifugation at 16,500 g for 10 min and protein concentrations were determined by BCA assay (Pierce). We obtained on average 1 mg of total protein per label out of 10 million cells. Cell lysates were mixed in equal protein amounts per label and proteins were reduced with 5 mM dithiothreitol and alkylated with 10 mM iodoacetamide. Samples were diluted 1:4 with HPLC water (Baker) and sequencing-grade modified trypsin (Promega, V5113) was added in an enzyme to substrate ratio of 1:150. After 16 h digest, samples were acidified with 0.5% trifluoroacetic acid (final concentration). Tryptic peptides were desalted on reverse phase tC18 SepPak columns (Waters, 500 mg, WAT036790) and dried in a vacuum concentrator centrifuge. Before phosphopeptide

enrichment peptides were separated using strong cation exchange (SCX) chromatography. Peptides were reconstituted in 500 µl strong cation exchange buffer A (7 mM KH<sub>2</sub>PO<sub>4</sub>, pH 2.65, 30% MeCN) and separated on a Polysulfoethyl A column from PolyLC (250 x 9.4 mm, 5 µm particle size, 200 Å pore size) using an Akta Purifier 10 system (GE Healthcare). We used an 80-min gradient with a 20-min equilibration phase with buffer A, a linear increase to 30% buffer B (7 mM KH<sub>2</sub>PO<sub>4</sub>, pH 2.65, 350 mM KCL, 30% MeCN) within 33 min, 100% B for 7 min and a final equilibration with Buffer A for 20 min. The flow rate was 3 ml/min and the sample was injected after the initial 20 min equilibration phase. Upon injection, 3 ml fractions were collected with a P950 fraction collector throughout the run. 60 fractions were collected of which 3-4 adjacent fractions were combined to obtain 12 samples. The 12 fractions were desalted with reverse phase tC18 SepPak columns (Waters, 100 mg, WAT036820) and lyophilized to dryness. SCX-separated samples were enriched for phosphopeptides by immobilized metal affinity chromatography (IMAC) as described previously (Chevrier et al., 2011). Peptides were reconstituted in 200 µl IMAC binding buffer (40% MeCN, 0.1% FA) and incubated for 1 h with 5 µl of packed Phos-Select beads (Sigma, P9740) in batch mode. After incubation, samples were loaded on C18 StageTips, washed twice with 50 µl IMAC binding buffer and washed once with 50 µl 1% formic acid. Phosphorylated peptides were eluted from the Phos-Select resin to the C18 material by loading 3 times 70 µl of 500 mM K<sub>2</sub>HPO<sub>4</sub> (pH 7.0). StageTips were washed with 50 µl of 1% formic acid to remove phosphate salts and eluted with 80 µl of 50% MeCN / 0.1 % formic acid. Samples were dried down by vacuum centrifugation and reconstituted in 8 µl 3% MeCN / 0.1 % formic acid. Peptide samples were separated on an online nanoflow HPLC system (Agilent 1200) and analyzed on a LTQ Orbitrap and a LTQ Orbitrap Velos instrument, as described (Chevrier et al., 2011). Briefly, 50% of the enriched phosphopeptide samples were loaded onto a 14-cm reverse



phase fused-silica capillary column (New Objective, PicoFrit PF360-75-10-N-5 with 10  $\mu\text{m}$  tip opening and 75  $\mu\text{m}$  inner diameter) packed in-house with 3  $\mu\text{m}$  ReproSil-Pur C18-AQ media (Dr. Maisch GmbH). The HPLC setup was connected via a custom-made electrospray ion source to the mass spectrometer. After sample injection, peptides were separated at an analytical flowrate of 200 nL/min with a 70-min linear gradient ( $\sim 0.29\%$  B/min) from 10% solvent A (0.1% formic acid in water) to 30% solvent B (0.1% formic acid/90% acetonitrile). The run time was 130 min for a single sample, including sample loading and column reconditioning. Data-dependent acquisition was performed using the Xcalibur 2.1 software in positive ion mode. Survey spectra were acquired in the orbitrap with a resolution of 60,000 and a mass range from 350 to 1750 m/z. In parallel, up to 16 of the most intense ions per cycle were isolated, fragmented and analyzed in the LTQ part of the instrument. Ions selected for MS/MS were dynamically excluded for 20 s after fragmentation.

### **Analysis of relative total protein expression**

BMDCs grown in SILAC media were left untreated or stimulated with LPS for 2 and 6 h. SILAC samples were lysed, digested and desalted as described for the global phosphoproteome analysis. To reduce sample complexity, 100  $\mu\text{g}$  of total peptides were separated using an Agilent 3100 Offgel fractionator (Agilent, G3100A) as described in the manual. For separation into 12 fractions, we used Immobiline DryStrips, 13cm, pH 3-10 (GE Healthcare, 17-6001-14) that were rehydrated in a 1:50 dilution of IPG buffer, pH 3-10 (GE Healthcare, 17-6000-87) containing 5% glycerol. Peptides were reconstituted in IPG buffer (1:50 dilution) containing 5% glycerol and focused for 20kV\*h with a maximum current of 50  $\mu\text{A}$  and power of 200 mW. After separation, fractions were acidified by adding 1% formic acid and desalted using StageTips. For global proteome analysis 1  $\mu\text{g}$  of peptide sample was separated on an online nanoflow HPLC system (Agilent 1200) and

analyzed on a LTQ Orbitrap and a LTQ Orbitrap Velos instrument, as described for the global phosphoproteome analysis of LPS timecourse samples.

### **Affinity purification followed by mass spectrometry (APMS) for V5-tagged MYD88, IRAK2 and AP1AR**

Analysis of interaction partners of V5-tagged proteins was performed using a fast and low-stringency single-step purification procedure (to retain weak binders and potentially transient interactions) as previously described (Hubner and Mann, 2011), with several modifications to fit our experimental system.  $2 \times 10^6$  bone marrow cells were plated in SILAC complete medium supplemented with 15 ng/mL GM-CSF in 10-cm Petri dishes, and infected two days later with lentiviruses (MOI ~10-20) containing V5-tagged ORFs (Yang et al., 2011) in 10-cm Petri dishes. 2-4 h after infection, cells were fed with GM-CSF-containing complete medium. Two days after infection, GM-CSF-containing complete medium supplemented with blasticidin (10 µg/mL) was added to cells, which were further incubated for 3 days. ORF expression and size was validated using standard Western blotting with anti-V5 antibody (Invitrogen). For immunoprecipitation (IP) of protein complexes, BMDCs expressing a V5-tagged ORF encoding human MYD88 (81.8% amino acid (AA) identity to mouse counterpart), IRAK2 (69.4% AA identity to mouse), or AP1AR (89.8% AA identity to mouse) were stimulated with LPS for 30 min, scraped on ice and washed in ice-cold PBS. Cell pellets were lysed for 30 min on ice in a lysis buffer containing 150 mM NaCl, 50 mM Tris pH 7.5, 5% Glycerol, 1% IGPAL-CA-630 (Sigma, #I8896), and freshly added protease and phosphatase inhibitors (Roche). After centrifugation at 4°C for 10 min at 14,000 g, protein concentration in supernatants was measured by BCA (Pierce), and equal amounts (~2.5-3 mg) of lysates from each SILAC sample were used for subsequent IP. Cell lysates were incubated

for ~16 h at 4°C on a roller with anti-V5 tag antibody covalently bound to magnetic beads (MBL). APMS experiments for MYD88 and IRAK2 were performed as on-bead digests with single-shot mass spectrometry runs, and the AP1AR interaction partners were analyzed by 8 slice in-gel digests with 8 LC-MS/MS runs. For MYD88 and IRAK2, beads were washed after anti-V5 immunoprecipitation twice with wash buffer (150 mM NaCl, 50 mM Tris pH 7.5, 5% Glycerol) containing 1% IGEPAL-CA-630, and twice with wash buffer alone. Beads from each SILAC state were combined after the first wash. Purified protein complexes were then eluted by direct on-bead digestion with trypsin using a buffer containing 2 M urea, 50 mM Tris pH 7.5, 1 mM DTT, and 5 µg/mL Trypsin. After elution, samples were reduced (4 mM DTT) and alkylated (10 mM iodoacetamide) following standard procedures, and further digested with trypsin overnight. Digestion were stopped by adding 1% TFA, and peptides were desalted purified on C18 StageTips before LC-MS/MS analysis. For AP1AR, anti-V5 enriched samples were washed three times with wash buffer and eluted from beads by heating to 100°C in SDS sample buffer (Life Technologies) for 5 min. Samples were separated on a 4-12% gradient gel (NuPAGE; Life Technologies) and cut into 8 slices that were subjected to in-gel trypsin digest and desalting on C18 StageTips as described previously (Lee et al., 2013). Desalted peptide samples for MYD88, IRAK2 and AP1AR APMS experiments were separated on an online nanoflow UHPLC system (Proxeon EASY-nLC 1000) and analyzed on a Q Exactive (Thermo Fisher Scientific) mass spectrometer. We used a 13-cm reversed phase fused-silica capillary column (New Objective, PicoFrit PF360-75-10-N-5 with 10 µm tip opening and 75 µm inner diameter) packed in-house with 3 µm ReproSil-Pur C18-AQ media (Dr. Maisch GmbH) and separated peptides at a flow rate of 200 nL/min in a 82 min linear gradient from 6 to 30% composition of solvent A (3% acetonitrile /0.1% formic acid) and solvent B (90% acetonitrile /0.1% formic acid). The Q Exactive was operated at a spray voltage of 2 kV,

a capillary temperature of 250 C and a S-lens RF level of 50. Data was acquired in positive ion mode, with MS1 scans at a resolution of 70,000 at  $m/z=200$ , a mass range of 300-1800, AGC target of  $1e6$  and 5 ms maximum ion time. Up to 12 of the most intense ions per duty cycle were isolated using an isolation window of 2.5  $m/z$  and fragmented by HCD at a NCE of 25 with an underfill ratio set at 5%. For data-dependent MS2 scans we used a resolution of 17,500, an AGC target of  $5e4$  and a maximum ion time of 120ms. All ions selected for MS2 scans were dynamically excluded for 20 s after fragmentation.

### **Massively parallel *in vitro* kinase (IVK) assay**

*In vitro* kinase reactions were performed with recombinant kinases on SILAC-labeled native cell lysates, as follows: 10 million cells were lysed in 1 ml of IVK lysis buffer (0.5% CHAPS, 50 mM Tris pH 7.5, 150 mM NaCl, 5 mM MgCl<sub>2</sub>, 5 mM MnCl<sub>2</sub>, 2 µg/ml Aprotinin (Sigma, A6103), 10 µg/ml Leupeptin (Roche, 11017101001) and 1 mM PMSF) for 20 minutes on ice to obtain a ~1 mg/ml protein lysate. Cell debris was removed by centrifugation for 15 minutes at 20,000 g and the protein concentration was measured using a Bradford assay. The buffer and low molecular weight components of the cell lysate were exchanged by size-exclusion chromatography using Zeba Spin Desalting Columns (Thermo Fisher Scientific, 89891, 5 ml column, 7K MWCO) at 4 C. The storage solution of the column was removed by centrifugation at 1,000 g for 2 minutes. The column was washed and equilibrated 4 times with 2.5 ml of ice-cold IVK reaction buffer (50 mM Tris pH 7.5, 150 mM NaCl, 5 mM MgCl<sub>2</sub>, 5 mM MnCl<sub>2</sub>, 0.5 mM DTT, 2 µg/ml Aprotinin (Sigma, A6103), 10 µg/ml Leupeptin (Roche, 11017101001) and 1 mM PMSF) by centrifugation at 1,000 g for 2 minutes. The column was then placed in a new collection tube, 1 ml of the IVK cell lysate was applied and the buffer exchanged by centrifugation at 1,000 g for 2 min. The column

flow-through contained cellular components of >7 kDa molecular weight in IVK reaction buffer. Before the in vitro kinase reaction phosphatase inhibitors were added as 1:100 dilutions of PIC2 (Sigma, P5726) and PIC3 (Sigma, P0044). For each IVK reaction 500 µg of SILAC-labeled total cellular proteins in IVK reaction buffer were used. Directly before the reaction, 1 mM of adenosine triphosphate (ATP) and 0.5 µg of recombinant kinase were added and the reaction was incubated for 1 h at 25 C. IVK reactions were performed for IRAK2 (SignalChem, I10-10BG), IRAK4 (EMD Millipore, 14-599), and TBK1 (EMD Millipore, 14-628). IVK reactions were stopped by adding 480 mg of urea per 500 µl of reaction buffer, resulting in a final concentration of 8M urea. Different SILAC samples for kinase and control (no kinase) reactions were combined, reduced with 5 mM DTT for 30 min, alkylated with 10 mM iodoacetamide for 30 min in the dark, diluted 1:4 with 50 mM Tris/HCl pH 7.5 and proteolytically digested with trypsin at a 1:50 enzyme to substrate ratio at 25 C for 16 h. The digests were acidified with 1% formic acid, precipitated urea was removed by centrifugation at 1,000 g for 10 min, and the samples were desalted using SepPak columns (Waters, 100 mg tC18, WAT036820). For single-shot IVK analysis samples were directly enriched for phosphopeptides by IMAC, whereas for deep coverage IVK analysis samples were separated into 6 basic reversed-phase (RP) fractions and then enriched by IMAC (see below).

### **Global phosphoproteome analysis of IVK samples and knock-out samples**

For IVK and KO phosphoproteome analysis desalted peptide samples were separated by basic reversed-phase (RP) prior to IMAC enrichment as described previously (Mertins et al., 2013). Total peptide amounts were 0.5 mg per SILAC state for IVK and 1.5 to 2 mg per SILAC state for wt and KO samples. For basic RP separation, desalted peptides were reconstituted in 900 µL of 20 mM ammonium formate, pH 10. Basic reversed-phase chromatography was performed on 4.6 mm

× 250 mm Zorbax 300 Å Extend-C18 columns (Agilent, 3.5 µm bead size), using an Agilent 1100 Series HPLC instrument. Prior to each separation, columns were monitored for efficient separation with standard mixtures containing 6 peptides. Solvent A (2% acetonitrile, 5 mM ammonium formate, pH 10), and a nonlinear increasing concentration of solvent B (90% acetonitrile, 5 mM ammonium formate, pH 10) were used to separate peptides by their hydrophobicity at a high pH. The flow rate was 1 ml/min and the percentage of solvent B was increased in a nonlinear gradient with 4 different slopes (0% for 9 min; 0% to 6% in 4 min; 6% to 28.5% in 50 min; 28.5% to 34% in 5.5 min; 34% to 60% in 13 min; 60% for 8.5 min). Eluted peptides were collected in 96 × 2 mL deepwell plates (Whatman, #7701-5200) with 1 min (= 1 ml) fractions. Early eluting peptides were collected in fraction “A”, which is a combined sample of all fractions collected before any major UV-214 signals were detected. Samples were combined into 6 or 12 subfractions, in a serpentine, concatenated pattern, combining every 12th fraction (1,13,25,37,...; 2,14,26,38,...; ...), or every 6th fraction (1,7,13,19,25,...; 2,8,14,20,26,...; ...). Subfractions were acidified to a final concentration of 1% formic acid and dried in a vacuum concentrator. For IMAC enrichment, iron-chelated IMAC beads were prepared from Ni-NTA superflow agarose beads (Qiagen, #1018611) that were stripped of nickel with 100 mM EDTA and incubated in an aqueous solution of 10 mM FeCl<sub>3</sub> (Sigma, 451649). Dried phosphopeptide fractions were reconstituted in 50% acetonitrile/0.1% trifluoroacetic acid and then diluted 1:1 with 100% acetonitrile/0.1% trifluoroacetic acid to obtain a final 80% acetonitrile/0.1% TFA peptide solution at a concentration of 0.5 µg/µl. Peptide mixtures were enriched for phosphorylated peptides with 10 µL IMAC beads for each sample for 30 min. Enriched IMAC beads were loaded on Empore C18 silica-packed Stage tips (3M, 2315). Stage tips were equilibrated with 2 × 100 µL washes of methanol, 2 × 50 µL washes of 50% acetonitrile/0.1% formic acid, and 2 × 100 µL washes of 1% formic acid. Samples were then loaded

onto stage tips and washed twice with 50  $\mu$ L of 80% acetonitrile/0.1% trifluoroacetic acid and 100  $\mu$ L of 1% formic acid. Phosphorylated peptides were eluted from IMAC beads with  $3 \times 70$   $\mu$ L washes of 500 mM dibasic sodium phosphate, pH 7.0, (Sigma, S9763) and washed twice with 100  $\mu$ L of 1% formic acid before being eluted from stage tips with 60  $\mu$ L 50% acetonitrile/0.1% formic acid. All washes were performed on a tabletop centrifuge at a maximum speed of 3,500g. Prior to LC-MS/MS analysis IMAC enriched samples were dried in a vacuum concentrator and reconstituted in 9  $\mu$ L of 3% ACN / 0.1% FA.

IMAC samples were analyzed on an online nanoflow EASY-nLC 1000 UHPLC system (Thermo Fisher Scientific) coupled to a benchtop Orbitrap Q Exactive mass spectrometer (Thermo Fisher Scientific). Fifty percent of each phosphopeptide sample were injected onto a Picofrit column (10  $\mu$ m tip opening / 75  $\mu$ m diameter, New Objective, PF360-75-10-N-5) packed in-house with 20 cm C18 silica material (1.9  $\mu$ m ReproSil-Pur C18-AQ medium, Dr. Maisch GmbH, r119.aq). The UHPLC setup was connected with a custom-fit microadapting tee (360  $\mu$ m, IDEX Health & Science, UH-753), and capillary columns were heated to 50  $^{\circ}$ C in column heater sleeves (Phoenix-ST) to reduce backpressure during UHPLC separation. Injected peptides were separated at a flow rate of 200 nL/min with a linear 80 min gradient from 100% solvent A (3% acetonitrile, 0.1% formic acid) to 30% solvent B (90% acetonitrile, 0.1% formic acid), followed by a linear 6 min gradient from 30% solvent B to 90% solvent B. Each sample was run for 150 min, including sample loading and column equilibration times. Data-dependent acquisition was obtained using Xcalibur 2.2 software in positive ion mode at a spray voltage of 2.00 kV. MS1 Spectra were measured with a resolution of 70,000, an AGC target of  $3e6$  and a mass range from 300 to 1800 m/z. Up to 12 MS2 spectra per duty cycle were triggered at a resolution of 17,500, an AGC target

of 5e4, an isolation window of 2.5 m/z and a normalized collision energy of 25. Peptides that triggered MS2 scans were dynamically excluded from further MS2 scans for 20 s.

### **Identification and quantification of phosphopeptides and proteins**

Mass spectra were processed within the Spectrum Mill (Agilent Technologies) and the MaxQuant (version 1.2.2.5) software packages (Cox and Mann, 2008) using a Uniprot mouse database containing 59,348 entries. The mass tolerance for precursor ions and for fragment ions was set to 20 ppm and 0.7 Da for LTQ-Orbitrap data and 20 ppm and 20 ppm for Q Exactive data, respectively. Cysteine carbamidomethylation was searched as a fixed modification, whereas variable oxidation on methionine and N-acetylation (Protein) was used for all analyzed datasets and phosphorylation on serine, threonine or tyrosine residues were considered as variable modifications for all phosphoproteome analyses. The enzyme specificity was set to trypsin and cleavage N-terminal of proline was allowed. The maximum of missed cleavages was set to 3. For peptide identification the maximum peptide FDR was set to 1%. SILAC ratios for phosphosites were obtained from the proteinPeptideComparisonColumnsExport table in Spectrum Mill and the Phospho (STY)Sites table in MaxQuant. The median ratios of all non-phosphorylated peptides derived from separate unmodified peptide exports in Spectrum Mill and MaxQuant were used to normalize the M/L and H/L ratios of all phosphorylated peptides and corresponding phosphosites. To allow better phosphosite grouping, Spectrum Mill and MaxQuant phosphosite annotations were converted to a unique identifier containing the uniprot accession number, the modified amino acid location and the number of phosphorylated residues on a peptide for each phosphosite quantification event. Median SILAC ratios of phosphopeptides for each experiment were calculated over all versions of the same peptide including different charge states and methionine



oxidation states. The highest scoring versions of each distinct peptide were reported per experiment. Data derived from both software packages was combined and Spectrum Mill data was reported when the same phosphopeptide was identified and quantified by both programs. Site-specific phosphosite localization scores were provided for both Spectrum Mill and MaxQuant. Lastly, only phosphosites that were observed in at least two independent SILAC experiments are reported.

### **Differential expression (DE) analysis of phosphoproteomic data**

To identify differentially regulated phosphosites in the time series, knockout, and IVK data sets, we used sets of 2 replicates of SILAC ratios for each experimental condition and filtered them to retain reproducible data. We deemed two ratios as reproducible if found within the 95% agreement limits of a Bland-Altman plot (Bland and Altman, 1986; Krönke et al., 2015). Then, we assessed statistical significance of differential phosphorylation using a moderated T-test (Smyth, 2004) and by correcting for multiple hypothesis testing using false discovery rate (FDR). When 2 replicates were not available, we proceeded as follows: (1) for the time series data, we paired 15- and 45-min samples with the corresponding, most correlated 30-min replicates (Pearson's correlation of 0.62 and 0.71 respectively); and (2) for the double knockout *Ticam*<sup>-/-</sup>*Myd88*<sup>-/-</sup> data, we used an absolute log2 fold-change threshold of 0.79 to filter phosphosites that were also asymmetrically differentially phosphorylated at 30 and 45 min in the time series data set. Lastly, for single KO datasets (*i.e.*, *Irak2*<sup>-/-</sup>, *Irak4*<sup>-/-</sup>, *Myd88*<sup>-/-</sup>), we focused our analyses on differentially regulated phosphosites that were also found to be (1) regulated in the time series data, and (2) affected by the double knockout *Ticam*<sup>-/-</sup>*Myd88*<sup>-/-</sup>.

### **Clustering of phosphoproteomic time series and candidate selection**

We performed supervised  $k$ -means clustering to partition the differentially expressed phosphopeptides from the time series experiment. We focused this analysis on phosphosites that were independently measured in 6 out of 8 time points, and showed differential regulation – based on the statistical criteria defined above – in at least 2 consecutive time points following LPS stimulation. We set the parameter  $k$  (number of clusters) as the minimal number of clusters that provided a sufficient level of within-cluster similarity. For every cluster, we define the within-cluster similarity as the average  $r^2$  between the members of the cluster and the centroid of the cluster. We used the following cutoffs for: the minimum within-cluster similarity (across all clusters) to be  $>0.7$ , and the average (across all clusters) to be  $>0.75$ . Using clustering and DE results, we selected 168 candidate phosphoproteins for genetic perturbations (**Figure 3**), including: (i) 121 that were both present in  $k$  clusters and differentially regulated in at least 2 consecutive, early time points (15 and 30 or 30 and 45 min); and (ii) 47 candidates manually added that were regulated in the same consecutive time points, but not measured in enough independent time points to pass the filters set prior to  $k$ -means clustering. Because several well-known TLR components (*e.g.*, TICAM1) were found to be strongly differentially regulated at early time points but were absent from the data at later time points, we reasoned that adding back several phosphoproteins showing a similar trend would alleviate some of the false negative problem associated with phosphoproteomic measurements.

### **Pathway enrichment analysis**

We measured enriched pathways in our data sets using DAVID (<http://david.abcc.ncifcrf.gov>), focusing on KEGG pathways and GO terms, and heatmaps were generated with Gene-E

(<https://software.broadinstitute.org/GENE-E/index.html>). Furthermore, to compile a gene set capturing most of the well described signaling and transcriptional regulators that have been implicated in the TLR pathways, we compiled a list of 141 genes (**Table S2**) by merging information from multiple databases: KEGG, InnateDB, Panther, Reactome, and Uniprot.

## **Integrative network analysis**

**Overview of the computational framework to identify signaling-to-transcription relationships.** To help uncover signaling-to-transcription relationships in the TLR4 system, we developed a computational framework to integrate biochemical datasets from this study and publicly available databases. First, we assembled a background interaction network combining protein-protein and kinase-substrate interactions (referred to as PPIs and KSIs, respectively) from several public repositories and augmented by adding APMS and IVK data from BMDCs. Second, we assigned weights to the edges (*i.e.*, PPIs, KSIs) and nodes (*i.e.*, signaling or transcriptional regulators) of this network to reflect prior knowledge and the biochemical changes affecting them based on our data sets (*i.e.*, differential phosphorylation upon LPS stimulation, kinase KO and IVK). Third, we searched for potential paths within the network that linked our 29 phosphoproteins ('seed nodes') to selected transcriptional regulators ('target nodes') and determined their significance using network randomization whereby weights were shuffled iteratively to compute statistical significance. We describe each step below.

**Step 1: Assembling the background interaction network.** We assembled an input set of interactions: 92,610 PPIs and 5,533 KSIs from public databases and AP-MS and IVK data sets from this study (**Table S7**). We collected the union of interactions found in mouse and/or human model systems in the following databases: (i) BioGRID (Stark et al., 2006), by keeping interactions

supported by at least one of the following experiments: Affinity Capture-Luminescence, Affinity Capture-MS, Affinity Capture-Western, Biochemical Activity, Co-crystal Structure, FRET, Far Western, PCA, Proximity Label-MS, Two-hybrid; (ii) PhosphoSitePlus (2014-09-03) (Hornbeck et al., 2015); and (iii) the Human Protein Reference Database (HPRD release 9) (Keshava Prasad et al., 2009), by focusing on interactions identified from two-hybrid experiments. Next, we filtered the resulting network by removing interactions with extracellular proteins (according to Swiss-Prot annotations) (Bairoch et al., 2004) and ubiquitously interacting protein modifiers (*i.e.*, *Ubc*, *Ubd*, *Sumo1*, *Sumo2*, *Sumo3*, *Nedd8*).

**Step 2: Defining seed-target relationship score.** First, we computed ‘relationship scores’ for each seed-target pair linked in the interaction network through at least one path (whereby a path represents a set of nodes and edges linking a seed to a target). The interaction network can be represented as a graph  $G=(V,E,w_n,w_e)$ , where  $V$  is a set of nodes (proteins),  $E$  is a set of edges (interactions), and  $w_n$  and  $w_e$  represent corresponding sets of weights assigned to nodes and edges respectively. The weight values were designed to be bigger than or equal to 0 but smaller than 1. Given a set of targets  $T \subset V$  and a set of candidate seeds  $A$ , we compute a ‘relationship score’  $S(A,T)=R$  (where  $R$  is a set of non-negative, real numbers). To do so, we take each simple path  $k$  from  $a \in A$  to  $t \in T$ , and assign to it a path score  $S_k = \prod_i w_{ni} * \prod_j w_{ej}$  where  $i$  and  $j$  go over all nodes and edges in the path. This score reflects the evidence that  $a$  interacts with  $t$  through the path  $k$ . Given that every path between  $a$  and  $t$  is increasing the total evidence that  $a$  influences  $t$  we compute the ‘relationship score’ as  $S(a,t) = \sum_k S_k$  where  $k$  enumerates all simple paths from  $a$  to  $t$  having at most 2 intermediate nodes. We note that in general, the longer the path, the smaller its score  $S_k$ .

**Step 3: Assigning weights to edges and nodes from the background interaction network.** First, to assign edge weights, we used two components: one to reflect the experimental evidence supporting a given PPI or KSI, and another to capture the local network topology as measured by the number of edges arriving to and leaving from a given node. The first component  $w_{e1}$  depended on the number  $n_{exper}$  of different experiment types supporting the interaction underlying a given edge (e.g., AP-MS, Y2H, etc.):

$$w_{e1} = 1 / (1 + e^{-2n_{exper}})$$

Therefore, the larger the number of experiment types  $n_{exper}$ , the higher the interaction weight. The second component  $w_{e2}$  depended on the local network topology: for an edge originating at node 1 and ending at node 2,  $nd_{out}$ ,  $nu_{out}$  are the numbers of all directed and undirected edges, respectively, originating at node 1, and  $nd_{in}$ ,  $nu_{in}$  the numbers of all edges ending at node 2. Then:

$$w_{e2} = \left[ \frac{1}{(0.5 * nd_{out} + nu_{out} + 1) * (0.5 * nd_{in} + nu_{in} + 1)} \right]^c$$

where the value of  $c = 0.01$ , was derived in the optimization step described below. The composite edge weight value  $w_e$  was set to  $0.9 * \sqrt[2]{w_{e1} * w_{e2}}$  for directed edges and  $0.45 * \sqrt[2]{w_{e1} * w_{e2}}$  for undirected ones. In addition, when an interaction was supported by AP-MS and/or IVK data from this study, we set the corresponding values of  $w_e$  to 0.999 and 0.99 for directed and undirected edges, respectively.

**Second, to assign node weights,** we first considered the background case, where differential phosphorylation information was not used. In this case, all network nodes were given

the same weight of 0.1, which maximized the performance on the following task: take KEGG pathway database (Kanehisa et al., 2016) (without ‘Toll-like receptor signaling pathway’), and use the transcription regulators as targets. Next, compute the seed-target relationship score for each possible seed-target pair. The pairs found to belong to the same KEGG pathway were then considered as true, and the pairs crossing the pathways as false (the intermediate nodes in network paths joining seed-target pairs were not restricted to KEGG proteins). The ‘relationship score’ depended on both the uniform node weight  $w_{n0}$  and the edge weights. Therefore, we concurrently searched for the optimal values of  $w_{n0}$  and parameter  $c$  (from the edge weight equation above) that maximized the area under the ROC curve. The resultant values for  $w_{n0}$  and  $c$  were 0.10 and 0.01, and they were used to define the ‘background network’ that is the input set of interactions with  $w_e$  and  $w_{n0}$ . Lastly, we reasoned that network nodes corresponding to differentially phosphorylated proteins in our experiments were more likely to transduce the signal from TLR4 to downstream gene regulation events. Therefore, for a given node  $i$  its weight  $w_{ni}$  increased with the number of experiments that indicated  $i$  as differentially phosphorylated:

<b>Data set</b>	<b><math>w_{ni}</math></b>	<b>Number of nodes</b>
Non-phosphorylated	0.10	8710
Time series (TS; 15, 30, 45 min)	0.20	1784
K-means	0.30	223
TS and double KO (dKO)	0.60	335
TS, dKO and 1 KO	0.63	302
TS, dKO and 2 Kos	0.67	217
TS, dKO and 3 Kos	0.70	31

(where TS stands for time series, KO stands for *Irak2*<sup>-/-</sup>, *Irak4*<sup>-/-</sup>, or *Myd88*<sup>-/-</sup>, and dKO for *Myd88*<sup>-/-</sup>/*Ticam1*<sup>-/-</sup> experiments). Resulting values  $w_{ni}$  were normalized such that their average was equal to 0.1 (*i.e.*, the same value as the uniform node weights  $w_{n0}$ ).

Resulting weights on network nodes defined the ‘weighted network’ that was used for ROC analysis (**Figure S7B**), as follows: (1) we used the set of known TLR components defined above (**Table S2**) and split it into targets (*i.e.*, transcriptional regulators) and seeds (*i.e.*, all other nodes). Furthermore, we focused on the 11 out of 14 TLR targets that were found as differentially phosphorylated in our time series phosphoproteomic data. (2) Seed-target pairs among the known TLR components were set as ‘true’, whereas pairs between TLR ‘targets’ and non-TLR ‘seeds’ present in the KEGG database set as ‘false’. (3) Lastly, we ordered seed-target pairs using only the sum of seed and target node weights as their relationship scores (*i.e.*, without using network paths scores). The corresponding ROC curve (‘phosphorylation only’) served as a reference benchmark for methods that used network information (**Figure S7B**).

**Step 4: Identify significant seed-target relationships.** We used bootstrapping to assign statistical significance of the ‘relationship scores’ computed above. To do so, we created 1000 randomized networks by swapping edges while keeping constant the node degrees (*i.e.*, the number of edges linking a given node) to maintain the network topology (Maslov and Sneppen, 2002). We randomized directed and undirected edges separately. The phosphorylation dependent node weights were randomly permuted among all nodes in the randomized networks. Next, ‘relationship scores’ between seeds and targets were computed in each random network. The resulting scores were used as a background distribution for empirical *p*-value computations. Specifically, we used marginal distributions, parametrized by the minimal path length. For example, if in the original non-randomized interaction network, a given seed was connected to its closest target by a path of

length  $l$ , then we used a distribution of relationship scores computed with paths of lengths bigger or equal  $l$ .

**Centrality score analysis.** After identifying significant seed-target pairs, we aimed to assign and compare the signaling centralities of the intermediate nodes (*i.e.*, excluding seed and target nodes) in each module of seeds (**Figures 3B and 5A**). For each module and each intermediate node, we summed scores of paths linking it with the corresponding set of significant seed-target pairs. This sum was then divided by the number of seeds in the module to arrive at the centrality score of an intermediate node in a module.

**Visualization of knockout effects seed-target relationships.** We quantified the effects of KO (*i.e.*  $Myd88^{-/-}$ ,  $Irak2^{-/-}$ ,  $Irak4^{-/-}$ ) on the ‘relationship scores’ of the significant (bootstrap  $p < 5 \times 10^{-4}$ , Benjamini-Hochberg FDR  $< 0.05$ ) seed-target pairs that were also affected by  $Myd88^{-/-}/Ticam1^{-/-}$ . For each simple seed-target path, we computed the percentage of the nodes affected by each KO. The total KO effect on a given seed-target pair was computed as the weighted average percentage from all paths, where weights were proportional to path scores  $S_k$ . The resulting KO effects were visualized using t-Distributed Stochastic Neighbor Embedding (t-SNE) (**Figure 7G**) and KOs with the weighted percentage of affected nodes bigger or equal to 50 were colored.



## SUPPLEMENTAL REFERENCES

- Bairoch, A., Boeckmann, B., Ferro, S., and Gasteiger, E. (2004). Swiss-Prot: juggling between evolution and stability. *Brief. Bioinformatics* 5, 39–55.
- Bland, J.M., and Altman, D.G. (1986). Statistical methods for assessing agreement between two methods of clinical measurement. *Lancet* 1, 307–310.
- Chevrier, N., Mertins, P., Artyomov, M.N., Shalek, A.K., Iannacone, M., Ciaccio, M.F., Gat-Viks, I., Tonti, E., DeGrace, M.M., Clauser, K.R., et al. (2011). Systematic discovery of TLR signaling components delineates viral-sensing circuits. *Cell* 147, 853–867.
- Cox, J., and Mann, M. (2008). MaxQuant enables high peptide identification rates, individualized p.p.b.-range mass accuracies and proteome-wide protein quantification. *Nature Biotechnology* 26, 1367–1372.
- Hornbeck, P.V., Zhang, B., Murray, B., Kornhauser, J.M., Latham, V., and Skrzypek, E. (2015). PhosphoSitePlus, 2014: mutations, PTMs and recalibrations. *Nucleic Acids Research* 43, D512–D520.
- Hubner, N.C., and Mann, M. (2011). Extracting gene function from protein-protein interactions using Quantitative BAC InteraCtomics (QUBIC). *Methods* 53, 453–459.
- Kanehisa, M., Sato, Y., Kawashima, M., Furumichi, M., and Tanabe, M. (2016). KEGG as a reference resource for gene and protein annotation. *Nucleic Acids Research* 44, D457–D462.
- Keshava Prasad, T.S., Goel, R., Kandasamy, K., Keerthikumar, S., Kumar, S., Mathivanan, S., Telikicherla, D., Raju, R., Shafreen, B., Venugopal, A., et al. (2009). Human Protein Reference Database--2009 update. *Nucleic Acids Research* 37, D767–D772.
- Krönke, J., Fink, E.C., Hollenbach, P.W., MacBeth, K.J., Hurst, S.N., Udeshi, N.D., Chamberlain, P.P., Mani, D.R., Man, H.W., Gandhi, A.K., et al. (2015). Lenalidomide induces ubiquitination and degradation of CK1 $\alpha$  in del(5q) MDS. *Nature* 523, 183–188.
- Lee, M.N., Roy, M., Ong, S.-E., Mertins, P., Villani, A.-C., Li, W., Dotiwala, F., Sen, J., Doench, J.G., Orzalli, M.H., et al. (2013). Identification of regulators of the innate immune response to cytosolic DNA and retroviral infection by an integrative approach. *Nat Immunol* 14, 179–185.
- Maritzen, T., Zech, T., Schmidt, M.R., Krause, E., Machesky, L.M., and Haucke, V. (2012). Gadkin negatively regulates cell spreading and motility via sequestration of the actin-nucleating ARP2/3 complex. *Proc. Natl. Acad. Sci. U.S.A.* 109, 10382–10387.
- Maslov, S., and Sneppen, K. (2002). Specificity and stability in topology of protein networks. *Science* 296, 910–913.
- Mertins, P., Qiao, J.W., Patel, J., Udeshi, N.D., Clauser, K.R., Mani, D.R., Burgess, M.W., Gillette, M.A., Jaffe, J.D., and Carr, S.A. (2013). Integrated proteomic analysis of post-translational modifications by serial enrichment. *Nat Meth* 10, 634–637.

Rehwinkel, J., Maelfait, J., Bridgeman, A., Rigby, R., Hayward, B., Liberatore, R.A., Bieniasz, P.D., Towers, G.J., Moita, L.F., Crow, Y.J., et al. (2013). SAMHD1-dependent retroviral control and escape in mice. *The EMBO Journal* 32, 2454–2462.

Smyth, G.K. (2004). Linear models and empirical bayes methods for assessing differential expression in microarray experiments. *Stat Appl Genet Mol Biol* 3, Article3–Article25.

Stark, C., Breitkreutz, B.-J., Reguly, T., Boucher, L., Breitkreutz, A., and Tyers, M. (2006). BioGRID: a general repository for interaction datasets. *Nucleic Acids Research* 34, D535–D539.

Yang, X., Boehm, J.S., Yang, X., Salehi-Ashtiani, K., Hao, T., Shen, Y., Lubonja, R., Thomas, S.R., Alkan, O., Bhimdi, T., et al. (2011). A public genome-scale lentiviral expression library of human ORFs. *Nat Meth* 8, 659–661.